

# Response of a single grafted polyethylene chain to simple shear flow: A Brownian dynamics simulation study

Turkan Haliloglu, Ivet Bahar, and Burak Erman

*Polymer Research Center and School of Engineering, Bogazici University and TUBITAK Advanced Polymeric Materials Research Center, Bebek 80815, Istanbul, Turkey*

(Received 31 January 1996; accepted 17 April 1996)

The behavior of a single polyethylene chain grafted to an impenetrable surface, under shear flow, is investigated using Brownian dynamics simulations. Both short-range conformational energies and excluded volume effects are included in the model. Simulations are performed in good and poor solvent conditions in order to explore the effect of solvent quality. The shear flow is represented by the superposition of a force profile increasing linearly with the distance from the surface. Distribution of rotational angles, chain dimensions, components of the radius of gyration, segment density distribution, average layer thickness, and average orientation of bond vectors with respect to flow direction are determined and compared with other studies. Above a certain value of the shear rate, a significant increase in chain dimensions is observed for both good and poor solvents, the transition from coiled to stretched state being sharper in poor solvent. In good solvent, chain dimensions along the two perpendicular directions to the flow direction diminish with increasing shear rate. On the other hand, in poor solvent, there is an overall expansion in chain dimensions in all directions at low shear rates, which is subsequently followed by the orientation and alignment of the chain along the direction of flow. The experimentally observed increase in chain dimensions normal to the flow field at low shear rates is evidenced for the first time by simulations. © 1996 American Institute of Physics. [S0021-9606(96)50428-9]

## INTRODUCTION

The behavior of polymer chains attached to a surface at one end and subject to a flow field is of significant interest for many practical applications such as steric stabilization, chromatography, tribology, etc. Knowledge of the conformations of end-grafted chains under shear flow is essential for improving the surface properties of the materials and predicting the surface and rheological properties of the chains in the above applications. The behavior of surface-bound chains has been studied (i) experimentally,<sup>1-5</sup> (ii) theoretically,<sup>6-14</sup> and (iii) by computer experiments. In the third group, some important problems of end-grafted polymers have been addressed using Monte Carlo (MC),<sup>15-17</sup> Brownian dynamics (BD),<sup>1,18-20</sup> and molecular dynamics (MD) simulations.<sup>21,22</sup> In the present BD simulation, the *equilibrium* properties of a single flexible end-grafted polyethylene (PE) chain under shear flow in different solvent regimes, below and above the  $\Theta$  state, are studied. The *dynamic* behavior of the chains under the same environmental conditions has also been investigated, and will be presented in a separate paper.

To date, the BD studies reported in the literature for terminally attached chains have been restricted to bead-spring<sup>1,18</sup> and freely jointed bead-rod model chains.<sup>20</sup> Although these simple models have been successful in giving insights into the general behavior of grafted chains, they were not completely successful in describing a number of experimental observations. Examples are the dependence of the stretch-coil transition phenomenon on the solvent quality, the shear induced expansion of the chain normal to the wall direction induced at low shear rates in poor solvent environment, etc. As will be shown below, the inclusion of the local

structural and conformational characteristics of real chains in the simulations permits assessment in detail, the response of end-grafted chains to the shear flow under different polymer-solvent interactions.

In the following sections, the simulation model and method will be described, and the response of the model chain to a wide range of shear rates in different solvent qualities will be analyzed.

## DESCRIPTION OF THE MODEL AND METHOD

The shear flow is implemented into the Brownian dynamics equation of motion by superposition of a force field parallel to the surface of adsorption, which increases linearly with separation from the surface. The equation of motion for the  $i$ th atom in a viscous medium in the presence of a random Brownian force and the external shear force takes the form

$$\beta d\mathbf{r}_i/dt = -\nabla_i U + \mathbf{F}_{si} + \mathbf{F}_{bi}(t). \quad (1)$$

Here,  $\beta$  is defined as the ratio  $\xi/m_i$  of the friction coefficient  $\xi$  and mass of the  $i$ th atom,  $m_i$ . In the present case,  $m_i \equiv m$  represents the mass of the unified  $\text{CH}_2$  groups, and the ratio  $\xi/m$  is taken<sup>23</sup> as  $10^5 \text{ ns}^{-1}$ .  $\nabla_i$  is the gradient operator indicating the partial derivative with respect to the position vector  $\mathbf{r}_i$ ,  $U$  is the total potential,  $\mathbf{F}_{bi}(t)$  is the Brownian force with zero mean and covariance  $\langle \mathbf{F}_{bi}(t) \mathbf{F}_{bj}(t') \rangle = 2\beta k_B T / m \delta_{ij} \delta(t-t') \mathbf{I}_3$ , where  $k_B$  is the Boltzmann's constant,  $T$  is the absolute temperature,  $\delta(t-t')$  is the Dirac delta function,  $\delta_{ij}$  is the Kronecker delta, and  $\mathbf{I}_3$

is identity matrix of order 3. The shear force is taken as  $\mathbf{F}_{si} = \beta \dot{\gamma}_0 z_i$ ,  $\dot{\gamma}_0$  being the zero shear rate, and  $z_i$  the distance of  $i$ th atom from the surface of adsorption.

The potential  $U$  includes bond angle bending, bond stretching, bond torsion potentials and Lennard–Jones (LJ) interactions. The latter is given by  $U_{LJ} = 4\epsilon[(\sigma/r)^{12} - (\sigma/r)^6]$ , if  $r < r_{\text{cut}}$ , and  $U_{LJ} = 0$  otherwise, for the chain units separated by four or more bonds along the backbone. Here,  $r$  is the distance between the interacting groups,  $\epsilon$  and  $\sigma$  are the energy and length parameters of the LJ potential.  $r_{\text{cut}}$  is the cutoff distance beyond which  $U_{LJ}$  is assumed to vanish. Hydrodynamic interactions are not taken into account. The solvent quality below and above the  $\Theta$  point is introduced by appropriate choices of  $\epsilon$  and  $r_{\text{cut}}$ . The value of  $r_{\text{cut}}$  is taken as  $2.5\sigma$  for poor solvent, and as  $2^{1/6}\sigma$  for good solvent conditions, i.e., intramolecular attractions cover a wider range in poor solvent environment.  $\sigma$  is taken as  $0.338\text{ nm}$ .<sup>24</sup> A value of  $0.5\text{ kJ/mol}$  is used for  $\epsilon$  under good solvent conditions; whereas the higher value of  $0.75\text{ kJ/mol}$  is adopted in poor solvent. This choice of cutoff and energy parameters ensures the occurrence of weaker attractions between chain units in good solvent, compared to those in poor solvent. The force constants<sup>25</sup> for bond angle bending, bond stretching, and torsional potentials are  $2.5 \times 10^9\text{ ns}^{-2}$ ,  $1.3 \times 10^7\text{ J/kg}$ , and  $6.634 \times 10^5\text{ J/kg}$ , respectively.

The PE chain has  $n = 100$  bonds of length  $l$ . The terminal atom is fixed in the  $xy$  plane, and the first bond is directed along the  $z$  axis. The bath temperature,  $T$ , is  $400\text{ K}$ . The time step of integration is taken as  $5\text{ fs}$ . The other simulation details and parameters may be found in our previous work.<sup>23,26,27</sup> Shear rate  $\dot{\gamma}_0$ , varied in the range  $0\text{--}85\text{ ns}^{-1}$ , is applied along the  $x$  direction. This range as will be shown below covers the passage from a coiled to a highly stretched conformation. The system is equilibrated for a relatively long duration (approximately  $10\text{ ns}$ ) prior to simulations. MD runs are carried out for  $10\text{ ns}$ , at least, for each choice of shear rate and solvent type.

## RESULTS

### Mean chain dimensions

In Fig. 1, snapshots of the chain configuration in poor solvent are shown at four different shear rates,  $\dot{\gamma}_0 = 0, 0.9, 4.3, 42.7\text{ ns}^{-1}$ . The effect of the shear flow along the  $x$  axis becomes rapidly significant and the chain obtains highly stretched conformations above  $\dot{\gamma}_0 = 4.3\text{ ns}^{-1}$ . At  $\dot{\gamma}_0 = 42.7\text{ ns}^{-1}$ , the chain has almost reached its fully extended configuration.

Figure 2 depicts the dependence of mean square end-to-end separation  $\langle R^2 \rangle$  on shear rate,  $\dot{\gamma}_0$  in poor (open circles) and good solvent (filled circles) regime. Figure 2(a) shows the logarithmic dependence of  $\langle R^2 \rangle$  on shear rate while Fig. 2(b) shows the normalized values of  $\langle R^2 \rangle$  where  $\langle R^2 \rangle_0$  and  $\langle R^2 \rangle_\infty$  are, respectively, the value of  $\langle R^2 \rangle$  in the quiescent solvent and under infinitely high shear rate. They are determined from the asymptotic values approached in the two limits in Fig. 2(a). BD results are connected by lines to guide the eye. The dotted straight lines on both sets of data of both

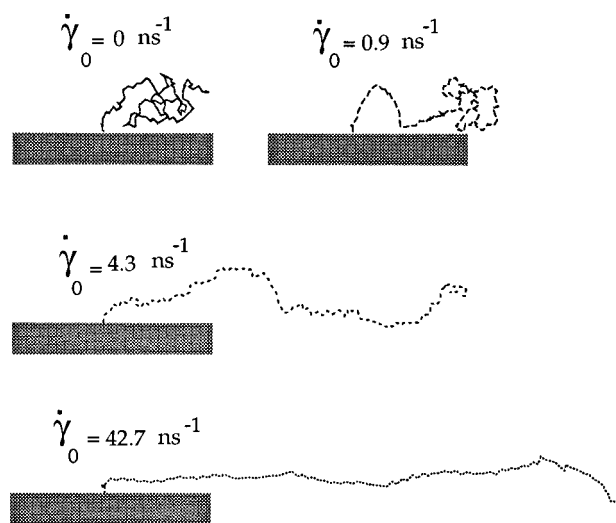


FIG. 1. Snapshots of the grafted chain in poor solvent, as projected on  $xz$  plane, under different shear rates, illustrating the gradual transition of the chain from coiled to stretched structure. The adsorption wall is given by  $xy$  plane. The chain configurations are shifted along the vertical axis for clarity.

figures represents the unperturbed dimensions that obtain in the absence of shear. The curves in Fig. 2(a) exhibit three distinct regions: For low values of  $\dot{\gamma}_0$  the chains are weakly deformed, and the coiled state persists. A sharp increase in chain dimensions in the range  $0.4 \leq \dot{\gamma}_0 \leq 4.0\text{ ns}^{-1}$  (approximately) is observed, characteristic of a transition between coil (C) and stretched (S) structures.

### Variation of conformer population and local geometry

The perturbation of the distribution  $P(\phi)$  of the backbone dihedral angles ( $\phi$ ) by the effect of the external shear force is presented in Fig. 3. Parts (a) and (b) are obtained for chains in poor and good solvent regimes, respectively. Curves labeled from  $i$  to  $v$  in the figures hold for the respective cases  $\dot{\gamma}_0 = 0, 0.9, 4.3, 21.4, 42.7\text{ ns}^{-1}$ . The population of *trans* conformers ( $\phi = 0^\circ$ ) increases with shear rate in both media. This is naturally accompanied by the depression of the probability of the *gauche*<sup>±</sup> ( $\phi = \pm 120^\circ$ ) states. On the other hand, for a given shear rate, the chain attains a relatively more extended conformation in good solvent regime, compared to poor solvent, as indicated by the lower probability values of the *trans* state (and higher probabilities of *gauche*<sup>±</sup> states) in Fig. 3(a).

In Fig. 4(a) the fraction,  $P_t$ , of *trans* conformers in poor solvent is presented as a function of  $\dot{\gamma}_0$ . The BD results are shown by the open circles and the curves are drawn for visualization. Here, the *trans* state is identified by dihedral angles in the range  $-40^\circ \leq \phi \leq +40^\circ$ . The dependence of the *trans* population on the shear rate reflects the response of the bond dihedral angles to the external field. Figures 4(b) and 4(c) illustrate the mean change in bond lengths and bond angles in response to the shear flow. The normalized mean-square bond length  $\langle L^2 \rangle$  and bond angle  $\langle \Theta^2 \rangle$  are plotted

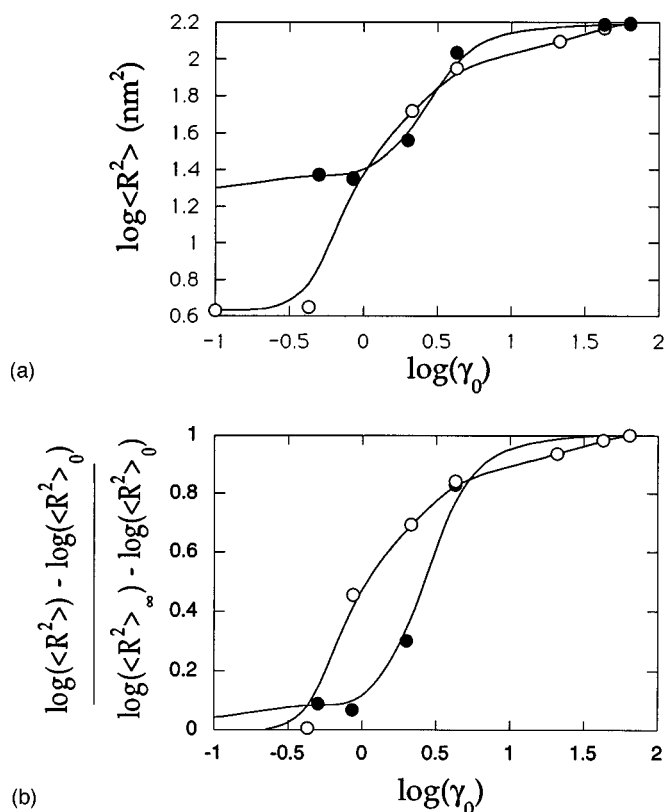


FIG. 2. (a) Dependence of the mean square end-to-end separation  $\langle R^2 \rangle$  of the grafted chain on shear rate, in good (filled circles) and poor (open circles) regimes obtained from BD simulations. The ordinate refers to the average taken over snapshots taken at 5 ps after equilibration of chain structure at a given shear rate. The curves through the are drawn to guide the eye. (b) Dependence of the normalized values of  $\langle R^2 \rangle$  on shear rate,  $\langle R^2 \rangle_0$  and  $\langle R^2 \rangle_\infty$  presents the value of  $\langle R^2 \rangle$  in the quiescent solvent and under infinitely high shear rate respectively, on shear rate, in good (filled circles) and poor (open circles) solvent regimes.

against  $\dot{\gamma}_0$  in parts (b) and (c), respectively. Here the BD results, shown by the open circles, are normalized in their full range of relaxation, so as to provide a quantitative comparison with the MC simulations of Lai *et al.*, shown by the open triangles in part (b). The absolute ranges in which the bond length and bond angles change upon stretching are  $0.1518 \leq l \leq 0.1575$  nm and  $110^\circ \leq \theta \leq 115^\circ$ , respectively, with the present choices of parameters.

The curve in part (a) of Fig. 4 is consistent with the transition observed at  $0 \leq \log \dot{\gamma}_0 \leq 1$  in Fig. 2, for the poor solvent case. In fact, an increase in the geometric variables is observable at higher shear rate. It is interesting to notice that, with increasing shear rate, the bond torsional angles are the first responding degrees of freedom. The changes in bond angles and bond lengths occur at somewhat higher shear rate, which is consistent with the fact that these degrees of freedom are stiffer than the bond torsional angles. Above shear rates of  $\dot{\gamma}_0 > \sim 60$  ns<sup>-1</sup>, the geometrical parameters assume values corresponding to complete unwinding of the coiled state. Yet, the coil (C)–stretch (S) transition occurs in the form of a second order transition rather than a discontinuous, first order transition. The occurrence of a C–S transition for

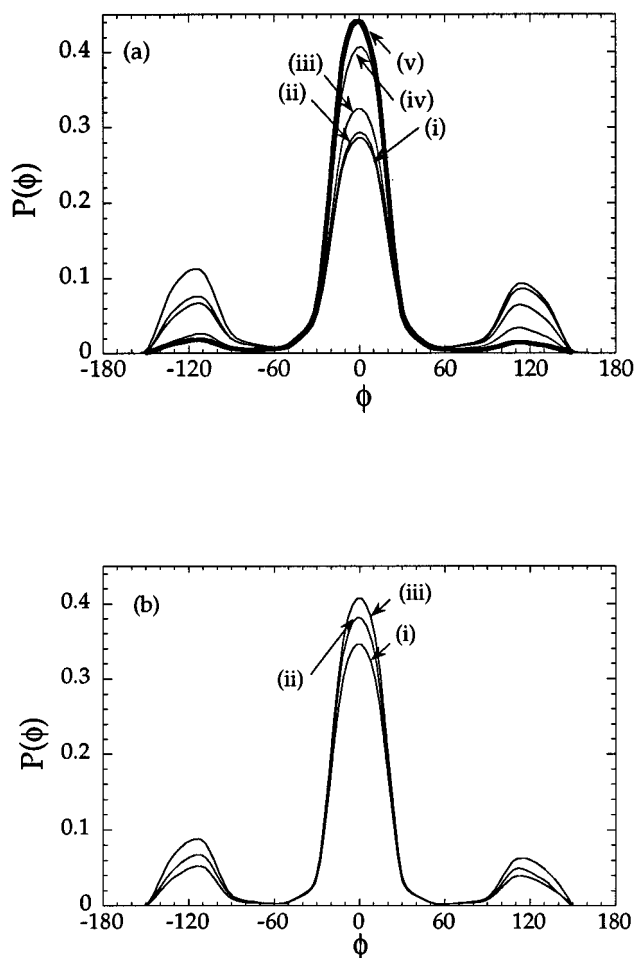


FIG. 3. Equilibrium distributions of bond dihedral angles,  $P(\phi)$ , in (a) poor solvent, and (b) good solvent obtained for (i)  $\dot{\gamma}_0=0$ , (ii)  $\dot{\gamma}_0=0.9$ , (iii)  $\dot{\gamma}_0=4.3$ , (iv)  $\dot{\gamma}_0=21.4$ , and (v)  $\dot{\gamma}_0=42.7$  ns<sup>-1</sup>. Increase in flow rate enhances the fraction of *trans* ( $\phi=0^\circ$ ) conformers and reduces that of *gauche*<sup>±</sup> conformers. The probability of the *gauche*<sup>±</sup> states is further depressed in good solvent.

the chains under flow was originally pointed out by de Gennes,<sup>10</sup> and applied to grafted chains under flow.<sup>11–13,28</sup>

### Components of the radius of gyration

Another statistical quantity useful in interpreting the results is the radius of gyration,  $R_g$ . Asymmetries in the conformations of the end-grafted chain resulting from its interaction with the flow can be clearly viewed in the  $x$ ,  $y$ , and  $z$  components of  $R_g$ . Figure 5 displays the components of the radius of gyration,  $\langle R_g x^2 \rangle^{1/2}$ ,  $\langle R_g y^2 \rangle^{1/2}$ , and  $\langle R_g z^2 \rangle^{1/2}$ , for poor (open circles) and good (filled circles) solvent regimes.

In good solvent,  $\langle R_g z^2 \rangle^{1/2}$  decreases with the shear rate, as expected from the alignment of chains parallel to the wall of adsorption due to flow. The changes in  $\langle R_g z^2 \rangle^{1/2}$  gradually level off above  $\dot{\gamma}_0=1$  ns<sup>-1</sup>, approximately, indicating that the chain tends to align parallel to the wall. A decrease in chain dimensions along the  $y$  direction is also observed, which is understandable from the fact that the flow field is applied along the  $x$  axis.  $\langle R_g x^2 \rangle^{1/2}$  increases with  $\dot{\gamma}_0$ , as ex-

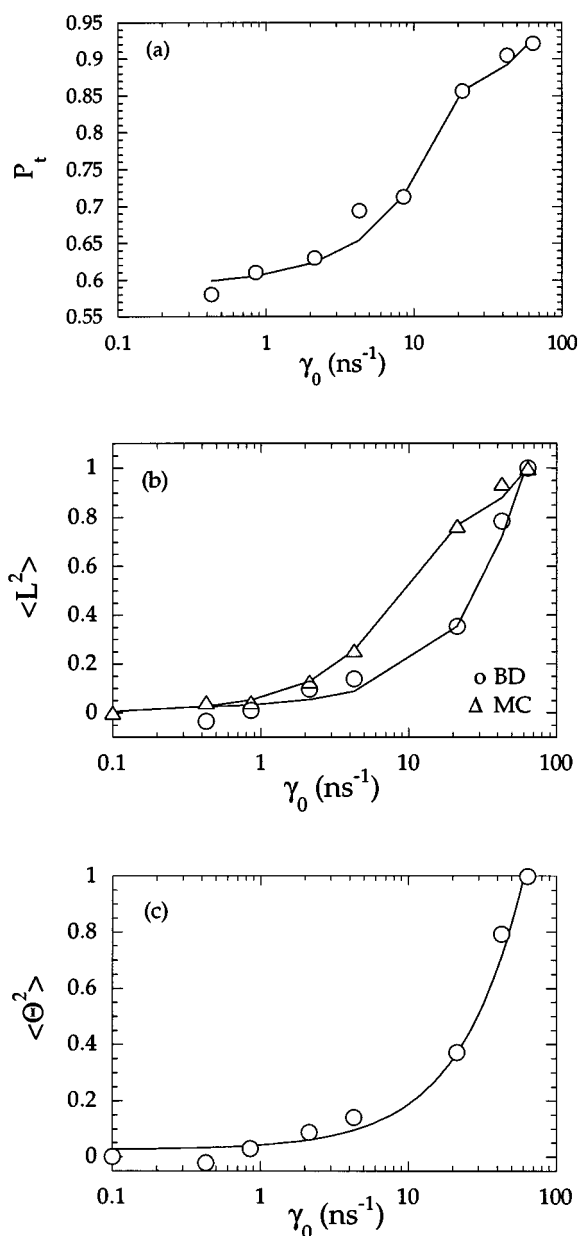


FIG. 4. (a) The fraction of *trans* conformers,  $P_t$  vs  $\dot{\gamma}_0$  for the chain in poor solvent. The increase in the population of *trans* rotameric states is particularly enhanced above  $\dot{\gamma}_0=10 \text{ ns}^{-1}$ . (b) The mean-square bond length  $\langle L^2 \rangle$ , normalized within the full range of the variable  $\langle l^2 \rangle$ , as a function of shear rate, in poor solvent. Triangles represent MC results of Lai *et al.* (c) The mean-square bond angle  $\langle \theta^2 \rangle$ , normalized with respect to the full range accessible to  $\theta$ , plotted against  $\dot{\gamma}_0$ .

pected. A unique sharp transition region is not discernible from the examination of the three curves:  $\langle R_{gz}^2 \rangle^{1/2}$  exhibits an abrupt decrease at  $\dot{\gamma}_0 \leq 0.4 \text{ ns}^{-1}$ . The response of  $\langle R_{gy}^2 \rangle^{1/2}$  is somewhat delayed to  $\dot{\gamma}_0 \approx 10 \text{ ns}^{-1}$ , whereas  $\langle R_{gx}^2 \rangle^{1/2}$  exhibits an intermediate behavior.

The behavior in poor solvent is completely different, except for high shear rates.  $\langle R_{gx}^2 \rangle^{1/2}$  shows a relatively sharp increase at about  $\dot{\gamma}_0=1 \text{ ns}^{-1}$ . It is interesting to notice that, at low shear rates ( $\dot{\gamma}_0 \leq 1 \text{ ns}^{-1}$ ) the stretching along the  $x$  axis is accompanied by the expansion of the chain in the  $z$  and  $y$

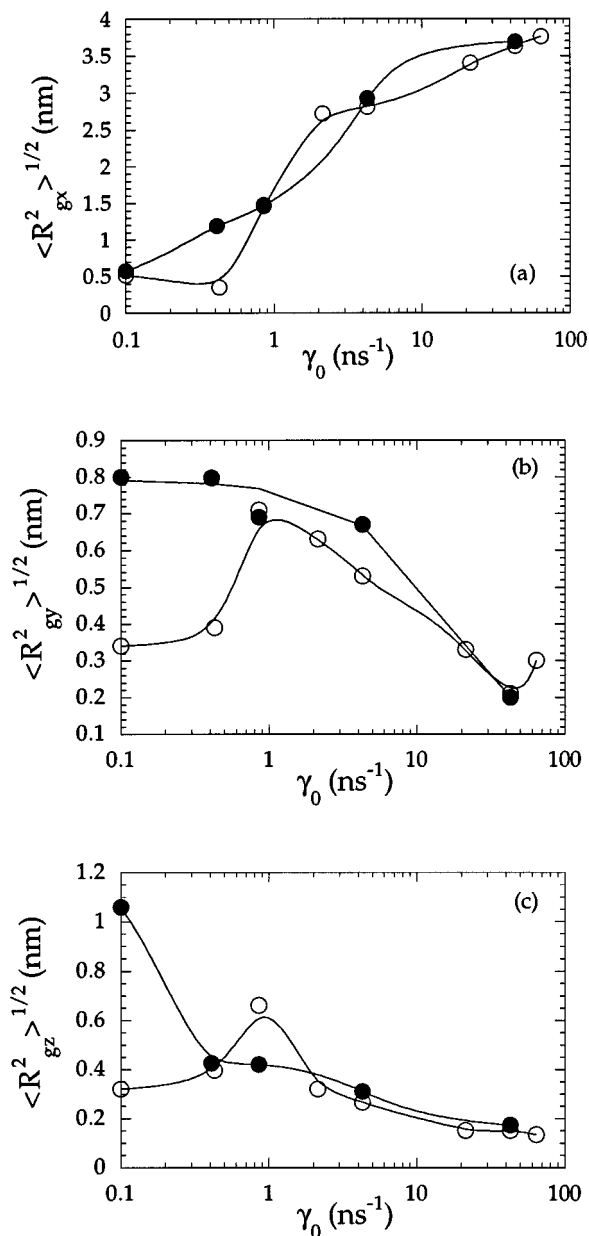


FIG. 5. Dependence of the components of the radius of gyration  $\mathbf{R}_g$  on the shear rate. The ordinate in parts (a), (b), and (c) represent the root-mean square components  $\langle R_{gx}^2 \rangle^{1/2}$ ,  $\langle R_{gy}^2 \rangle^{1/2}$ , and  $\langle R_{gz}^2 \rangle^{1/2}$  of  $\mathbf{R}_g$ . Open and filled circles stand for the results in poor and good solvent, respectively.

directions, as well. An inversion in chain dimensions along the  $z$  and  $y$  directions is observed at  $\dot{\gamma}_0=1 \text{ ns}^{-1}$ , approximately, which is followed by the contraction of the  $y$  and  $z$  components of the radius of gyration. This phenomenon was verified by several independent runs. The increase in the components of the radius of gyration along the two perpendicular directions to the flow field, at low shear rate and under poor solvent conditions, is a unique phenomenon conforming with experimental evidence.<sup>5</sup> In fact, a shear-induced expansion of the adsorbed polymer layer is observed by Cohen<sup>5</sup> in the study of polystyrene-cyclohexane in  $\theta$  conditions at low shear rates. The concentration of the polymer

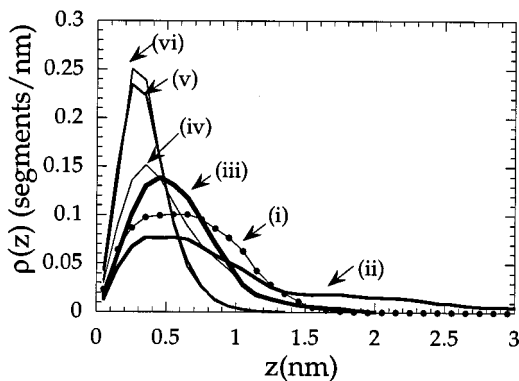


FIG. 6. Distribution of number density of chain segments  $\rho(z)$ , as a function of the distance from the adsorption surface,  $z$ . Layers of thickness  $\Delta z=0.01$  nm are observed at various snapshots under a given flow field for determining  $\rho(z)$ . Curve (i) represents the distribution in the absence of flow. Curves (ii)–(vi) are obtained for the respective cases of 0.9, 2.1, 4.3, 21.4, and 42.7  $\text{ns}^{-1}$ .

adsorbed on the surface in that experiment was low enough to validate the comparison of these experimental observations with the present results obtained for a single grafted chain. The rise in the thickness of the adsorbed layer below the critical shear rate is attributed,<sup>5</sup> to the shear-induced disentanglement of subloops and/or the detachment of the trains from the surface. The occurrence of this phenomenon is demonstrated for the first time by BD simulations.

We note that similar calculations have been carried out in a recent MC study<sup>17</sup> of a single grafted chain, and BD simulation of a single grafted chain of freely jointed bead rods.<sup>20</sup> There, it was not possible to observe the effect of the solvent quality.

### Surface density distribution and mean layer thickness

The density distribution of chain segments  $\rho(z)$  under different shear rates in poor solvent are displayed in Fig. 6, as a function of the vertical separation  $z$  from the wall. The ordinate  $\rho(z)$  represents the average number of  $\text{CH}_2$  units located in successive layers of thickness 0.1 nm, starting from the interface. The curves are drawn for the cases (i)  $\dot{\gamma}_0=0$ , (ii)  $\dot{\gamma}_0=0.9 \text{ ns}^{-1}$ , (iii)  $\dot{\gamma}_0=2.1 \text{ ns}^{-1}$ , (iv)  $\dot{\gamma}_0=4.3 \text{ ns}^{-1}$ , (v)  $\dot{\gamma}_0=21.4 \text{ ns}^{-1}$ , and (vi)  $\dot{\gamma}_0=42.7 \text{ ns}^{-1}$ .

In general, the distributions obey a Gaussian-type form which becomes narrower, and shifts towards smaller  $z$  values with increasing shear rate. In the highest value of  $\dot{\gamma}_0=42.7 \text{ ns}^{-1}$ , chain units are practically confined to a region of thickness  $\sim 0.75$  nm, with a highest density at 0.25 nm.

On the other hand, at low shear rates, the density distribution of chain units becomes broader than that of the free ( $\dot{\gamma}_0=0$ ) chain, as may be seen from the comparison of the curves (i) and (ii). This shear-induced expansion of the adsorbed layer is consistent with the initial (at low  $\dot{\gamma}_0$ ) expansion of the  $z$  component of the radius of gyration in poor solvent, already shown in Fig. 5(c). An inversion in the dependence of  $\rho(z)$  on the shear rate occurs at about  $\dot{\gamma}_0=1.0 \text{ ns}^{-1}$ , as already apparent in Figs. 5(b) and 5(c). Beyond this

TABLE I. Average layer thickness  $\langle L_z \rangle$  for grafted chain under shear flow.

$\dot{\gamma}_0$ ( $\text{ns}^{-1}$ )	Poor solvent $\langle L_z \rangle$ (nm)	Good solvent $\langle L_z \rangle$ (nm)
0	0.65	2.04
0.4	0.80	
0.9	0.76	0.78
2.1	0.54	
4.3	0.52	0.58
21.4	0.35	
42.7	0.35	

value, the distribution curves indicate a gradual concentration of chain units within regions closer to the wall with increasing flow rate.

The average height of the layer occupied by chain segments may be estimated either from the first moment of the density profile or from the average position of the last atom in the chain. Table I shows the layer thickness,  $\langle L_z \rangle$ , evaluated from the first moments as a function of shear rate in both good solvent and poor solvent conditions. The responses of the chain in the two different types of solvents are quite different, as already revealed in the preceding figures. At lower shear rates, an increase in the shear rate leads to an increase in layer thickness in poor solvent, whereas the latter decreases uniformly in good solvent.

At low values of shear rate in poor solvent the chain segments unfold, which were originally in a relatively contracted configuration due to unfavorable interaction with the solvent. At stronger shear rates, as the chain is expanded and oriented along the flow, the chain segments gradually approach the wall, in both solvents. Upon further increase of the shear rate, a new regime is entered, where the bond angles and bond lengths deform appreciably. This resembles the above mentioned experimental observation of Cohen.<sup>5</sup> We note that experiments carried out by Klein and co-workers<sup>4</sup> suggest that shear flow in fact increases the brush thickness. Another experimental study by Lee *et al.*<sup>1</sup> revealed that in polystyrene samples at the  $\Theta$  temperature, no detectable changes in the layer thickness were obtained, except for the one with the highest molecular weight where a decrease in layer thickness took place.

### Local and global orientation of the chain with respect to the flow field

The *local* orientation of chain segments with respect to the direction of the flow may be evaluated from the average cosine of the angle  $\alpha$  between the bond vectors and the direction of flow as

$$S(z) = \frac{1}{2} [3 \langle \cos^2 \alpha(z) \rangle - 1]. \quad (2)$$

Here,  $S(z)$  is the order parameter which represents the average orientation of chain segments located at an elevation  $z \pm \Delta z$  from the wall. The angular brackets refer to the ensemble average over all bonds in that particular layer of thickness  $\Delta z$ , and time average over several snapshots of

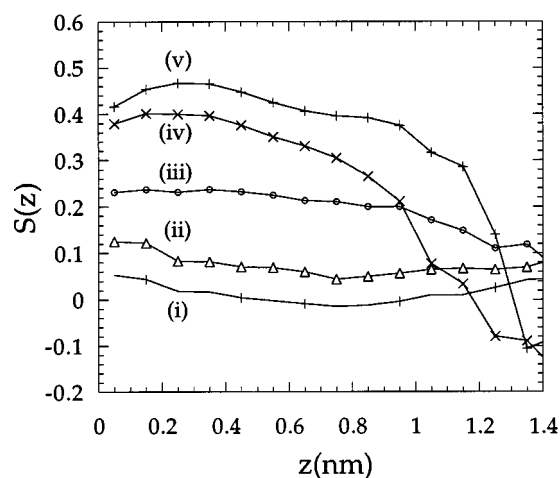


FIG. 7. The order parameter  $S(z)$  for bond vectors located at an elevation  $z \pm \Delta z$  from the wall, in poor solvent under different shear rates. Curve labels (i)–(v) refer to the respective cases of 0, 0.9, 4.3, 21.4, and 42.7  $\text{ns}^{-1}$ .

interval 5 ps. The results obtained for PE chains subject to various strength flow fields in poor solvent are illustrated in Fig. 7. Curves (i)–(v) refer to shear rates of  $\dot{\gamma}_0 = 0, 0.9, 4.3, 21.4$  and  $42.7 \text{ ns}^{-1}$ , respectively.  $\Delta z$  is taken as 0.1 nm. In the absence of shear flow  $S(z)$  is approximately zero for all  $z$ , indicating no preferential orientation. With the application of flow field, a gradual reorientation along the direction of flow takes place. This response is more evident at small separations  $z$  from the wall; whereas bonds located farther from the wall exhibit a weaker reorientation. The order parameter sharply decreases with  $z$  at higher shear rates.

An assessment of the degree of orientation of the overall chain with respect to the direction of the flow field may be made on the basis of the angular deviation between the flow direction and the mean chain direction. The mean chain direction is defined by the unit vector  $\mathbf{e}_{\text{cm}}$  directed from the first atom to the mass center of the chain. The inclination of  $\mathbf{e}_{\text{cm}}$  with respect to the flow direction is expressed in terms of the angle  $\Psi = \cos^{-1}(\mathbf{e}_{\text{cm}} \cdot \delta_x)$  where  $\delta_x$  is the unit vector in the direction of flow. Figure 8 shows the time average  $\langle \cos \Psi \rangle$  as a function of  $\dot{\gamma}_0$  for the two types of solvents. At high shear rates ( $\dot{\gamma}_0 \geq 5 \text{ ns}^{-1}$ ) the chain is almost fully aligned along the flow direction; further extension of the chain is imparted by the distortion of bond lengths and angles, and does not affect the global reorientation. The chain in good solvent (filled circles) exhibits a weaker dependence on the shear rate than that in poor solvent (open circles). For comparison, results obtained by Lai *et al.*<sup>17</sup> by lattice MC simulations of a single grafted chain are also displayed in the figure by the open triangles. An important feature is the occurrence of a smoother transition in MC simulations, whereas the present BD simulations indicate a rather sharper passage, in poor solvent particularly, from random to fully oriented chain structure.

#### FURTHER INTERPRETATION OF RESULTS AND COMPARISON WITH OTHER WORK

An interesting feature observed from the snapshot of the chain for  $\dot{\gamma}_0 = 0.85 \text{ ns}^{-1}$  is a “flowerlike” configuration,<sup>13</sup>

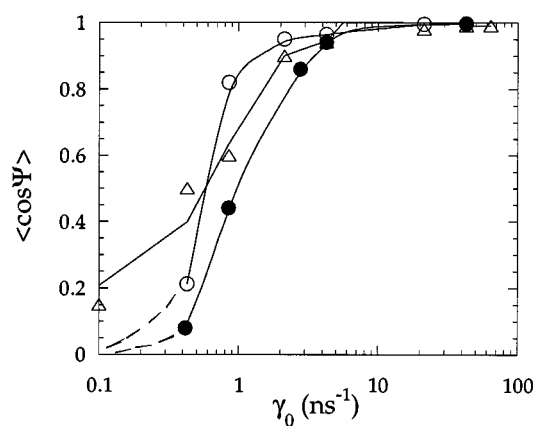


FIG. 8. Dependence of the global chain orientation on shear rate. The ordinate  $\langle \cos \Psi \rangle$  represents the average cosine of the angle  $\psi$  between the flow direction and the mean chain direction. BD results are shown for the poor solvent (filled circles) and good solvent (open circles). Triangles represent the results from the MC simulations of Lai *et al.* (Ref. 17).

where a number of bonds starting from the one attached to the wall are in a highly oriented and extended configuration (*stem* part) and the remaining ones up to the free end of the chain are in a relatively disordered state (*flower* part). This is in agreement with the recent predictions of Brochard-Wyart.<sup>13</sup> It is to be noted that at higher flow rates, the flowerlike configuration is lost and the so-called *stem* part of the chain grows, and eventually all bonds become strongly oriented. The flowerlike configuration is intuitively plausible because the stem is subject to a large shear force and is expected to orient strongly while the bonds at the free end enjoy a high mobility and therefore assume a relatively disordered state.

In poor solvent, the onset of the transition region is observed in Figs. 2 and 8 to take place at  $\dot{\gamma}_0 = 0.5 \text{ ns}^{-1}$ , approximately. This value may be rationalized in terms of the dimensionless parameter  $\dot{\gamma}_0 \tau_z$  where  $\tau_z$  is the Zimm relaxation time for weak perturbations<sup>13</sup> and is given by the relation

$$\tau_z = \frac{\eta R_F^3}{kT}. \quad (3)$$

Here  $\eta$  is the solvent viscosity related to the friction coefficient  $\xi$  by the Stokes law,  $\xi = 6\pi\eta a$ . In the latter expression,  $a$  is the hydrodynamic radius of a  $\text{CH}_2$  group.  $R_F$  in Eq. (3) is the Flory radius of the chain. With these expressions, one obtains the relaxation time as

$$\tau_z \sim \left[ \frac{\xi/kT}{6\pi a} \right] (C_\infty n^{2\nu} l^2)^{3/2}, \quad (4)$$

where the exponent  $\nu$  is  $3/5$  for a good solvent and  $1/3$  for a poor solvent.  $C_\infty$  is the characteristic ratio which is equal to 6.4 for PE chains of 100 bonds. At the onset of the transition region, one would expect this dimensionless number  $\dot{\gamma}_0 \tau_z$  to equate to unity. Substitution of the values corresponding to our system, i.e.,  $n = 100$ ,  $l = 0.153 \text{ nm}$ ,  $a = 0.076 \text{ nm}$ ,  $\xi/m = 10^5 \text{ ns}^{-1}$ ,  $T = 400 \text{ K}$  leads to a correlation time  $\tau_z$  of

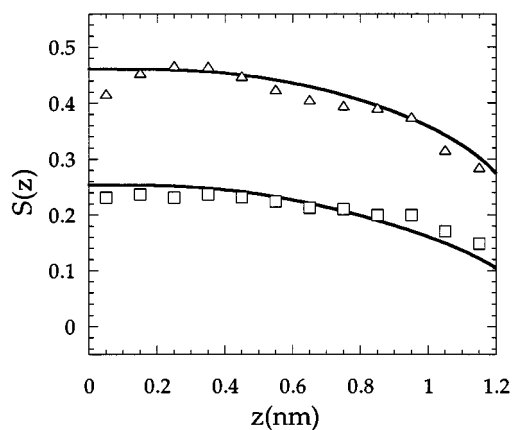


FIG. 9. The order parameter  $S(z)$  for bond vectors located at an elevation  $z \pm \Delta z$  from the wall, calculated from BD simulation, in poor solvent at  $\dot{\gamma}_0 = 4.3$  ( $\square$ ), and  $42.7$  ( $\triangle$ )  $\text{ns}^{-1}$ . The bold face solid curves are calculated using Eq. (8).

1.68 ns in poor solvent. Equating the dimensionless number to unity leads to a shear rate of  $\dot{\gamma}_0 = 0.6 \text{ ns}^{-1}$  in agreement with the results obtained by BD simulations. However, we note that in good solvent, Eq. (5) predicts a larger  $\tau_z$ , and consequently lower  $\dot{\gamma}_0$ , which is in qualitative disagreement with simulations.

The segment density distribution curves shown in Fig. 6 may be expressed by a distribution of the form

$$\rho(z) = A \exp[-az]z^2, \quad (5)$$

where  $A$  is the normalization constant,

$$A = \frac{2}{a^3} \left\{ 1 - \exp(-aL_{\max}) \left[ \frac{(aL_{\max})^2}{2} + aL_{\max} + 1 \right] \right\} \quad (6)$$

provided that the  $\rho(z)$  is normalized in the finite interval  $[0, L_{\max}]$ . Here,  $L_{\max}$  is taken as the fully extended length of the chains. The values of the parameter  $a$ , may be readily obtained by a least square fit to the distribution functions of Fig. 6, whereas the choice of the upper bound  $L_{\max}$  has negligibly small effect provided that the latter is sufficiently large. On the other hand, the orientation function  $S(z)$  given in Fig. 7 may be approximated by a relation of the form

$$S(z) \sim f(z)^r = K' \left[ \int_z^L z \rho(z) dz \right]^r, \quad (7)$$

where  $f(z)$  is the total force experienced by a chain unit at the level  $z$ ,  $K'$  is a proportionality constant, and  $r$  is an exponent. Substituting Eq. (5) in Eq. (7), we obtain a proportionality of the form

$$S(z) \sim \left[ \int_z^L z^3 \exp(-az) dz \right]^r. \quad (8)$$

The values for  $S(z)$  for the two curves, (iii) and (v), of Fig. 7 were calculated by using Eq. (8). The value of the exponent  $r$  giving the best fit was obtained as  $1/4$ . The results of calculations are illustrated by the two boldface curves in Fig. 9 and compared with corresponding results of BD simulations.

## CONCLUDING REMARKS

The differences in the behavior of the polymer chain in the two types of solvent vanish with increasing flow rate. The most severe departure between the response of the chain in the two different media to a flow field is observed at low shear rates. The major difference is the following: In poor solvent, the flow field first expands the chain, and subsequently deforms it along the preferred direction. The increase in chain dimensions at low shear rates is evidenced in parts (b) and (c) of Fig. 5. Likewise, the probability distributions in Fig. 6 and the layer thicknesses obtained at various shear rates (Table I) confirm the same behavior. Such an inversion is not observed in good solvent, where the lateral (with respect to flow field) components of the radius of gyration are strictly decreasing with  $\dot{\gamma}_0$ .

The passage from coiled to stretched state is observed to be sharper and faster in poor solvent compared to that in good solvent. This feature is indicated by the curves in Fig. 2 and 8. We note that, in agreement with the present results, the stretching of a collapsed coil is observed by MC simulations<sup>29</sup> to exhibit an abrupt upturn of the force-length curve, which is explained as a transition of a globular coil into an extended coil. A smoother passage occurs in good solvent.

Tirrell and collaborators report that no apparent shear-induced expansion of adsorbed layers takes place in pure shear flow unless there exists some local flow perpendicular to the adsorption surface, induced by wall roughness.<sup>3</sup> In the present simulations, inhomogeneities in the flow field are introduced by the Brownian character of the polymer motion. In other words, polymer segments are subject to a pure shear force and a random force, simultaneously. This may partly explain the expansion of chain dimensions in the directions transverse to that of the flow field at low shear rates.

It should be noted that this observation was only possible upon the use of real structure and energy characteristics of the polymer chain, which was not explicitly accounted for in previous BD simulations.

An interesting point concerns the response of the chain orientation on a local scale to the externally applied flow field. Although a linear dependence of  $S(z)$  on the applied force  $f(z)$  might be expected by analogy to segmental orientation of a uniaxially deformed chain which is not bound to any surface,<sup>30</sup> a weaker dependence is observed in the presently investigated grafted chains under shear flow. A relationship of the form  $S(z) \sim f(z)^{1/4}$  is estimated from the analysis of the density distribution functions and bond orientations as a function of the separation from the adsorption surface.

## ACKNOWLEDGMENTS

Partial supports provided by National Science Foundation Grants Project No. INT 9312285, and by Bogazici University Research Funds Project No. 95P003 are gratefully acknowledged.

- <sup>1</sup>J.-J. Lee and G. G. Fuller, *Macromolecules*, **17**, 375 (1984).  
<sup>2</sup>H. J. Taunton, C. Toprakcioglu, L. J. Fetters, and J. Klein, *Nature* **332**, 712 (1988).  
<sup>3</sup>M. Bagassi, G. Chauveteau, J. Lecourtier, J. Englert, and M. Tirrell, *Macromolecules* **22**, 262 (1989).  
<sup>4</sup>J. Klein, D. Perahia, and S. Warburg, *Nature* **352**, 143 (1991).  
<sup>5</sup>Y. Cohen, *Macromolecules* **21**, 494 (1988).  
<sup>6</sup>S. T. Milner, *Science* **251**, 905 (1991).  
<sup>7</sup>J.-L. Barrat, *Macromolecules* **25**, 832 (1992).  
<sup>8</sup>Y. Rabin and S. Alexander, *Europhys. Lett.* **13**, 49 (1990).  
<sup>9</sup>S. T. Milner, *Macromolecules* **24**, 3704 (1991).  
<sup>10</sup>P. G. de Gennes, *J. Chem. Phys.* **60**, 5030 (1974).  
<sup>11</sup>F. Brochard-Wyart and P. G. de Gennes, *Langmuir* **8**, 3033 (1992).  
<sup>12</sup>F. Brochard-Wyart, *Europhys. Lett.* **23**, 105 (1993).  
<sup>13</sup>F. Brochard-Wyart, *Europhys. Lett.* **30**, 387 (1995).  
<sup>14</sup>T. T. Perkins, D. E. Smith, R. G. Larson, and S. Chu, *Science* **268**, 83 (1995).  
<sup>15</sup>E. Duering and Y. Rabin, *Macromolecules* **23**, 2232 (1990).  
<sup>16</sup>P.-Y. Lai and K. Binder, *J. Chem. Phys.* **97**, 586 (1992).  
<sup>17</sup>P.-Y. Lai and K. Binder, *J. Chem. Phys.* **98**, 2366 (1993).  
<sup>18</sup>E. A. Dimarzio and R. J. Rubin, *J. Polym. Sci: Polym. Phys. Ed.* **16**, 457 (1978).  
<sup>19</sup>I. M. Neelov and K. Binder, *Macromol. Theory Simul.* **4**, 119 (1995).  
<sup>20</sup>R. S. Parnas and Y. Cohen, *Macromolecules* **24**, 4646 (1991).  
<sup>21</sup>K. Kremer and G. S. J. Grest *Chem. Phys.* **92**, 5057 (1990).  
<sup>22</sup>M. Murat and G. S. Grest *Macromolecules* **22**, 4054 (1989).  
<sup>23</sup>T. Haliloglu, I. Bahar, and B. Erman, *J. Chem. Phys.* **97**, 4428 (1992).  
<sup>24</sup>P. R. Sundararajan and P. J. Flory *J. Am. Chem. Soc.* **96**, 1117 (1974).  
<sup>25</sup>E. Helfand, Z. R. Wasserman, and T. A. Weber, *Macromolecules* **13**, 526 (1980).  
<sup>26</sup>T. Haliloglu, B. Erman, and I. Bahar, *J. Chem. Phys.* **97**, 4438 (1992).  
<sup>27</sup>T. Haliloglu, I. Bahar and B. Erman, *Polymer* **34**, 440 (1993).  
<sup>28</sup>V. G. Mavrantzas and A. N. Beris, *J. Rheol.* **36**, 175 (1992).  
<sup>29</sup>P. Cifra and T. Bleha, *Macromol. Theory Simul.* **4**, 233 (1995).  
<sup>30</sup>J. E. Mark and B. Erman, *Rubberlike Elasticity. A Molecular Primer* (Wiley-Interscience, New York 1988).